Korean Journal of Geomatics
Vol. 4, No. 1 / November 2004
pp. 1~8

Sub-Pixel Analysis of Hyperspectral Image Using Linear Spectral Mixing Model and Convex Geometry Concept

Dae-Sung KIM*, Yong-Il KIM and Young-Jae LIM*****

Abstract

In the middle-resolution remote sensing, the Ground Sampled Distance (GSD) that the detector senses and samples is generally larger than the actual size of the objects (or materials) of interest, and so several objects are embedded in a single pixel. In this case, as it is impossible to detect these objects by the conventional spatial-based image processing techniques, it has to be carried out at sub-pixel level through spectral properties. In this paper, we explain the sub-pixel analysis algorithm, also known as the Linear Spectral Mixing (LSM) model, which has been experimented using the Hyperion data. To find Endmembers used as the prior knowledge for LSM model, we applied the concept of the convex geometry on the two-dimensional scatter plot. The Atmospheric Correction and Minimum Noise Fraction techniques are presented for the pre-processing of Hyperion data. As LSM model is the simplest approach in sub-pixel analysis, the results of our experiment is not good. But we intend to say that the sub-pixel analysis shows much more information in comparison with the image classification.

Keywords : *Hyperspectral Image, Minimum Noise Fraction(MNF), Convex Geometry, Linear Spectral Mixing (LSM) Model, Sub-Pixel Analysis, Endmember*

1. Introduction

If Remote Sensing images have high spatial resolution, objects can be detected with the spatial and spectral information. But if not, it is impossible to detect the object embedded in a pixel. Therefore one of the greatest challenges in hyperspectral imaging is performing the sub-pixel analysis, which is typically not treated in standard spatial-based image processing.

The Linear Spectral Mixing (LSM) model (Settle, 1996) is one of the most important approaches in sub-pixel analysis performed on hyperspectral datasets. This approach comprise of two processes; finding spectrally unique signatures of pure ground components (usually referred to as endmembers) and expressing individual pixels as linear combination of endmembers (Antonio, 2002). Here, we adopted the concept of the convex geometry involving the representation of the set of all scene pixels as a two-dimensional scatter plot in spectral space. We also introduce the general techniques for LSM model. Before discussing the details of this research, we would like to make two statements: 1) the analysis of hyperspectral data, as well as multispectral data, is an important process for Remote Sensing; and 2) the sub-pixel analysis with high-dimensional data provides more effective information in comparison with the image classification.

This paper is organized as follows. Section II provides an overview of Hyperspectral Remote Sensing. Section III describes the fundamental principle of the proposed approach. Section IV illustrates our method based on the experimental result. Finally, Section V provides some conclusions and comments on future research.

2. Hyperspectral Remote Sensing

Hyperspectral Remote Sensing (also known as Imaging Spectrometry, Imaging Spectroscopy or

*Ph. D. Candidate, School of Civil, Urban, and Geosystem Eng., Seoul National University (E-mail : mutul94@empal.com)
**Associate Professor, School of Civil, Urban, and Geosystem Eng., Seoul National University (E-mail : yik@snu.ac.kr)
***Researcher, Spatial Information Research Team, Telematics Research Division, ETRI (E-mail : yjlim@etri.re.kr)

The manuscript for this paper was submitted for review on August 19, 2004 / accepted on September 20, 2004

Hyperspectral Imaging) is defined as "the acquisition of imagers in hundreds of registered, contiguous spectral bands such that for each pixel of an image it is possible to derive a complete reflectance spectrum (Goetz, 1992; Freek, 2001)". Hyperspectral images take advantage of the hundreds of contiguous spectral channels to uncover materials that usually cannot be resolved by multispectral sensors. Fig. 1 explains the concept of hyperspectral Remote Sensing that acquires the information on the interested area and provides a reflectance spectrum for every pixel in the hyperspectral data.

Hyperspectral imaging is a fast growing area in Remote Sensing (Chang, 2003). During the last several years, a great number of new airborne and spaceborne hyperspectral sensors have been improved for hyperspectral remote sensing applications. At the present time, acquisition of airborne hyperspectral image is limited by instrument availability and cost. Probe 1 (128 channels, 0.44~2.50㎛), Hymap (Hyperspectral Mapping System, 126 channels, 0.45~2.50㎛) and HYDICE (Hyperspectral Digital Imagery Collection Experiment, 210 channels, 0.40~2.50㎛) are commercially available, while other instruments such as AVIRIS (Airborne and Infra-Red Imaging Spectrometer, 224 channels, 0.40~2.50㎛) are available to only NASA-supported researchers (Antonio, 2002). The Hyperion on EO-1 satellite is known to be the first commercial spaceborne hyperspectral sensor and the data can be available at low cost services from USGS or TRW.

There are numerous specialized methods for analyzing high-dimensional data. For example, Binary Encoding is a classification method that encodes the image data and reference spectra into 0s and 1s based on whether a band falls below or above the spectrum mean (Mazer, 1988). The Spectral Angle Mapper matches pixel spectra to reference spectra using a measure of spectral similarity based on the angle between the spectra treated as vectors in an N-dimensional space (Kruse, 1993). Spectral Feature Fitting uses least squares methods to compare the fit of image spectra to selected reference spectra (Clark, 1990). Matched Filtering method performs a partial unmixing of spectra to estimate the abundance of user-defined endmembers from a set of reference spectra (Harsanyi and Chang, 1994). In addition to the above analysis techniques that are applied on hyperspectral data, there are many other researches, including ourselves, who are developing new techniques.

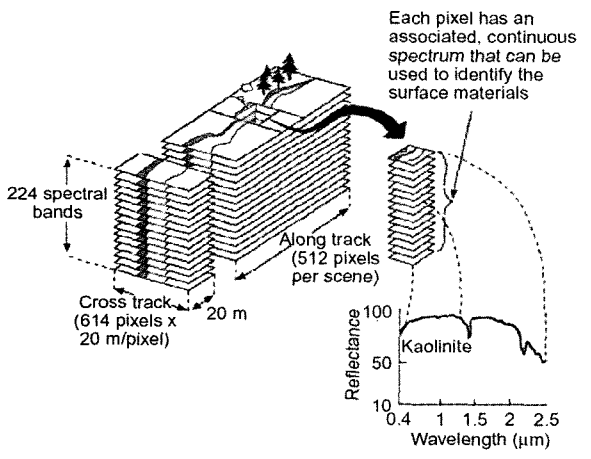

Fig. 1. Concept of Hyperspectral Remote Sensing (Freek, 2001).

3. Sub-Pixel Analysis

The main objective of sub-pixel analysis methods is to identify the relative contribution of different materials to the spectral composition of a given pixel. This means that the high-dimensionality of the hyperspectral data takes advantage of sub-pixel analysis to identify sub-components of the spectrum for each pixel (Richard, 2002). The main algorithms for sub-pixel analysis are Matched Filtering, Mixture Tuned Matched Filtering and LSM model. Among these, the LSM model is described below and has been applied to Hyperion data in practice.

3.1 Linear Spectral Mixing Model

A pixel observed by the remote sensing instrument consists of mixed materials. Therefore, the LSM model, intended for determining the relative abundances of materials that are depicted in multispectral or hyperspectral image depending on the materials' spectral characteristics, is used to resolve this spectral mixing problem.

In the LSM model, the spectrum of a mixed pixel is represented as a linear combination of component spectra. The weight of each endmember spectrum is proportional to the fraction of the pixel area (abundance) covered by the endmember (Dimitris, 2000). Therefore, the general equation for mixing by area is given by

$$x = \sum_{k=1}^{M} s_k a_k + w \quad (1)$$

Where,

x : spectrum of the mixed pixel

s_k : spectra of the endmembers
a_k : abundances
M : the number of endmembers
w : N - dimensional error vector for lack-of-fit

Physical considerations dictate the following constrains which can be enforced to guarantee meaningful parameter values.

$$1 \geq a_k \geq 0, \quad \sum_{k=1}^{M} a_k = 1 \tag{2}$$

If Eq. (1) is expanded, the pixel value matrix of N-dimension is as follows.

$$_N X_1 = {}_N S_M \, {}_M A_1 + {}_N W_1 \tag{3}$$

Where, $M < N$

Using the Least Square method, we can get the value of abundance from Eq. (4).

$$A = (S^T S)^{-1} S^T X \tag{4}$$

3.2 Endmember Extraction

Given the endmember spectra, the LSM model finds out the abundance values of each endmember for every pixel. Since the results of LSM model are highly dependent on the input endmembers and the change of endmembers, the determination of the endmember is an important step.

A number of algorithms based on the notion of spectral mixture modeling have been proposed over the past decade to perform the complex task of finding appropriate endmembers for LSM model in hyperspectral data. One of the most successful approaches is the Pixel Purity Index (PPI), which is based on the geometry of convex sets. There are other attempts that have been made recently processed to extract endmembers such as N-FINDR, ORASIS (Optical Real-time Adaptive spectral identification System), IEA (Iterative Error Analysis), and MESMA (Multiple Endmember Spectral Mixture Analysis).

The convex geometry was applied to the endmember extraction technique in this study. Convex geometry deals with the geometry of convex sets, where a convex set in N-dimensions is defined as a set of points that are linear combinations of some set of points of which the weights are all positive and sum to unity. This is also the same definition used for the LSM model. A

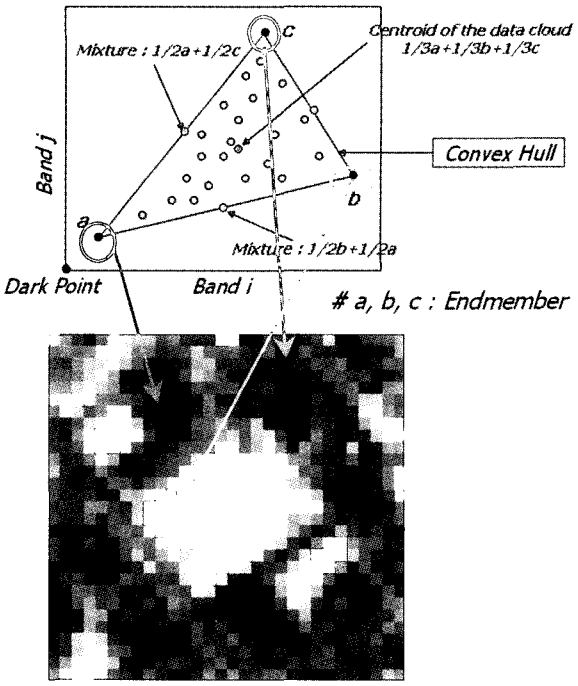

Fig. 2. Concept of the Convex Geometry for Linear Mixture (above) and Extracted Endmembers from 2D scatter plot (case 2, below).

body made up of N+1 points is the simplest possible, that has some interior, and is called a simplex (Boardman, 1993).

We selected the 3 endmember classes manually on the two-dimensional space. The band combination for this two-dimensional scatter plot was determined by values of correlation coefficient between bands. Fig. 2 illustrates the concepts of Convex Geometry for linear mixture and the endmembers extracted by this method correspond to some pixels (2～4 pixels per endmember) in the subset image.

4. Experiments

4.1 Data

The simple processing in sub-pixel analysis with LSM model is shown in Fig. 3.

To demonstrate LSM model, the Hyperion data which are sensed by EO-1 satellite was used. The Earth Observing (EO-1) Satellite was launched on November 21, 2000 as the first Earth observing platform of NASA's New Millennium Program (NMP). The EO-1 satellite contains three observing instruments, Advanced Land Imager (ALI), LEISA Atmospheric Corrector (LAC), and Hyperion Imaging Spectrometer, supported by a variety of newly developed space technologies. The basic specification of the EO-1 sensors is given in Table 1.

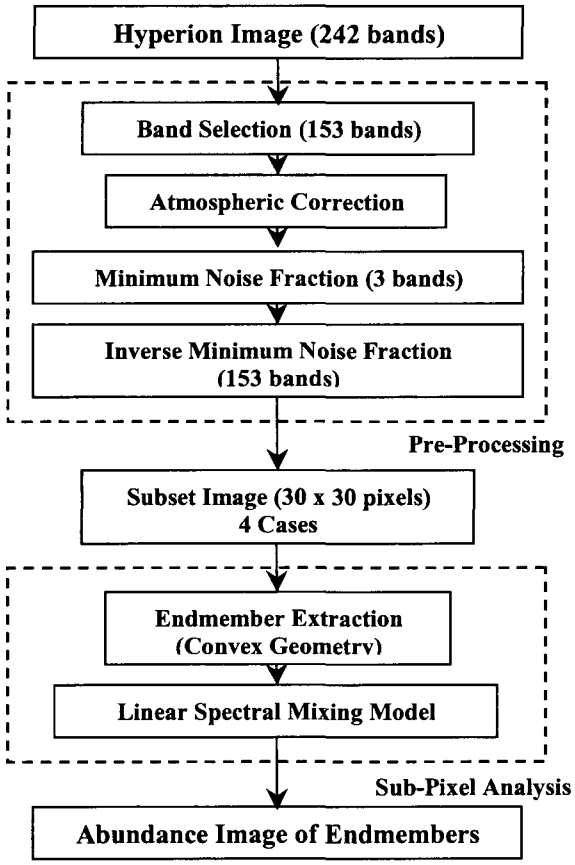

Fig. 3. Flow Chart of Sub-Pixel Analysis.

Table 1. Specification of EO-1 Sensors.

Parameters	Hyperion	ALI	LAC
Swath Width	7.6km	37km	185km
Spatial Resolution	30m	30m	250m
Channels	220	10	256
Spectral Range	0.4~2.5㎛	0.4~2.5㎛	0.9~1.6㎛

As the number of endmembers that can be extracted in a two-dimensional space is 3, the subset images of 4 cases that are composed of about 3 objects were used in applying the LSM model to the hyperspectral data. The image size was 30×30 pixels and study area was situated in An-Yang, Korea (Fig. 4).

4.2 Pre-processing

To pre-process for Hyperion data, Atmospheric Correction and Minimum Noise Fraction (MNF) techniques were applied. The MNF transformation is used to determine the inherent dimensionality of image data, to segregate noise in the data, and to reduce the computational requirements for subsequent processing (Boardman, 1994). The MNF transformation is essentially two cascaded Principal Components (PC) transformation. Among the images transformed by MNF, 3 bands were extracted by using the eigenvalues and the existing data were restored to 153 bands through Inverse MNF transformation.

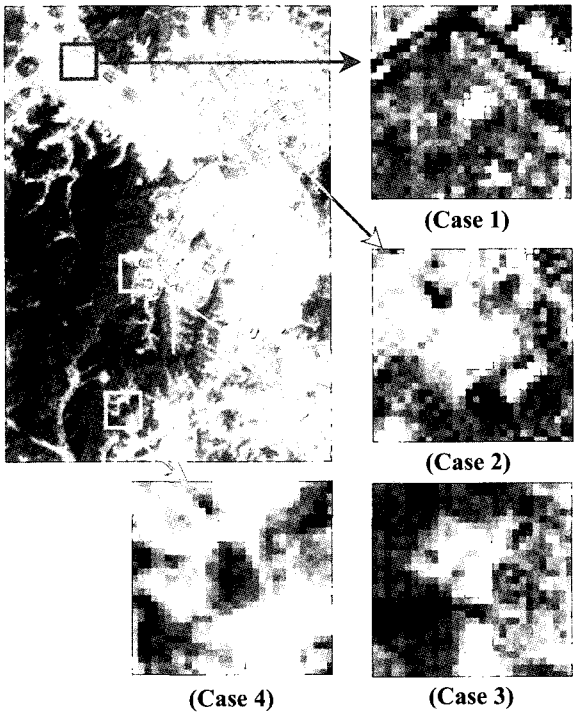

Fig. 4. Study Area (R: 30, G: 20, B: 10).

Atmospheric Correction is an essential step that must be performed, because the effects of the atmosphere must be removed in order for image spectra to match library spectra. But it may not be required with field mapping to train the image. In this processing, Internal Average Relative Reflectance (IARR) was applied for reducing the effects of the atmosphere. IARR normalizes images to a scene's average spectrum. This is particularly effective for reducing hyperspectral data to relative reflectance in an area where no ground measurements exist and little is known about the scene (Kruse, 1985).

4.3 Band Combination and Class Index

The values of correlation coefficient between bands were used to combine the bands for 2-D scatter plot on the spectral space. All subset images were calculated statistically and two of them were selected with the lowest correlation coefficient. Fig. 5 shows the example image of the correlation coefficient. The bands combined in the subset image and their coefficients are arranged in Table 2.

3 Endmembers extracted on the 2-D spectral space

Fig. 5. Example of Correlation Coefficient Image (Case 3, 153 153 pixels).

Table 2. Band Combination and the Lowest Correlation Coefficients between Bands.

	Case 1	Case 2	Case 3	Case 4
Band Combination	3 and 64	3 and 64	15 and 64	3 and 64
Correlation coefficient	0.295	0.632	0.009	0.337

were simply indexed through a map drawn on a scale of 1 to 25,000. (Case 1 - water, soil, and manmade; Case 2 - grass, soil, and manmade; Case 3 - forest, soil (or bright concrete), and manmade; Case 4 - forest, grass, and water)

4.4 Results

The results of spectral mixing appear as a series of gray-scale images, one for each endmember, plus a RMS error image. Higher abundances (and higher errors for the RMS error image) are represented by the brighter pixels (larger floating-point numbers). We can also find areas with missing or incorrect endmember in the RMSE image. If the RMS error doesn't become less than before error, the LSM model is completed.

In general, two constraints, sum-to-one and non-negative, should be imposed on the LSM model to produce a desired solution. These have already been described before (see the Eq. (2)). We did not obtain satisfactory results from the LSM model were not satisfied in practice because the convex geometry was not perfect. This means that the outer pixels do influence the result as the pixels plotted in the two-dimensional spectral space are not in the convex hull. To resolve this problem, we adjusted the values of abundance through a simple calculation in sum-to-one and non-negative.

Some of the results of the LSM model display are displayed below. For the visual estimation, the result images were processed to 2% linear stretch and we represented each result in a three-dimensional block diagram. Fig. 6 is the abundance images of endmember which show the best results for each case. As you can see, the results show that LSM model is effective in analyzing soil (case 1, 2, and 3) or water (case 4). But since these are unique groups of endmembers compared with the other endmembers, it seems to be much easier to acquire a good endmember class. Figures 7~10 presents the abundance value of 30×30 pixels in a three-dimensional block diagram. The x-axis and y-axis are the image coordinates and whereas the z-axis shows the calculated abundance value. It should be noted that if the value is greater (or the length of the block is longer), there is relatively higher possibilities of endmember existing while if the value is lower, the opposite trend would be observed.

For the quantitative approach, the highest and lowest values of abundance from the LSM, and their image coordinates are arranged in the Tables 3 and 4. The values of the RMSE are generally low, but this means only the difference between the initial values for calculation and the result values, which depends on the endmember classes that are selected in the beginning.

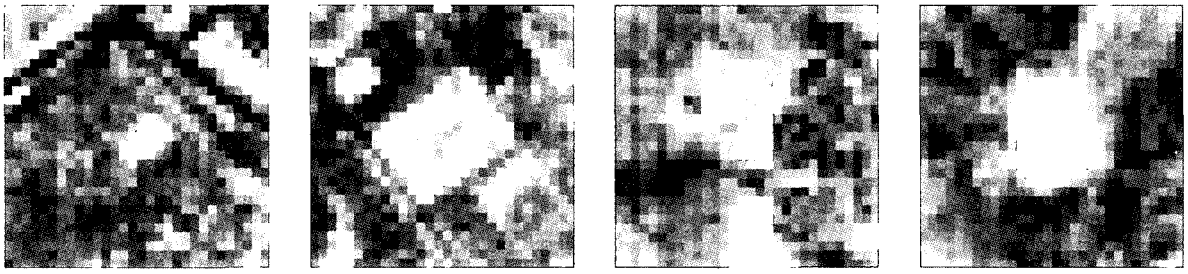

(a) Case 1 (Soil) (b) Case 2 (Soil) (c) Case 3 (Bright Concrete) (d) Case 4 (Water)

Fig. 6. Abundance Images of the Best Results for Each Case.

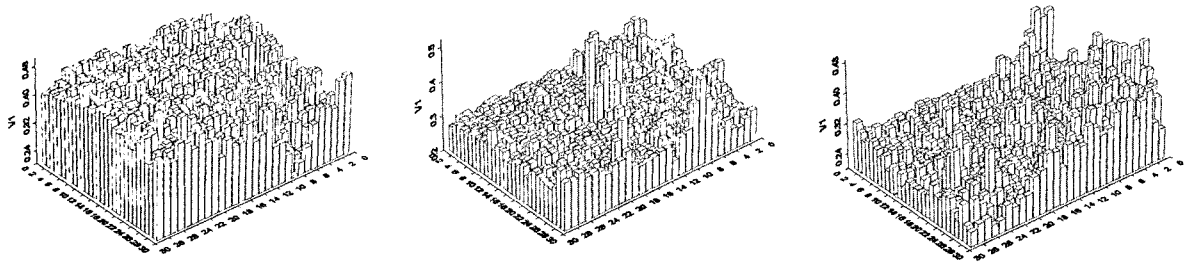

Fig. 7. Three-Dimensional Block Diagram of Case 1 (left: Water, middle: Soil, right: Manmade).

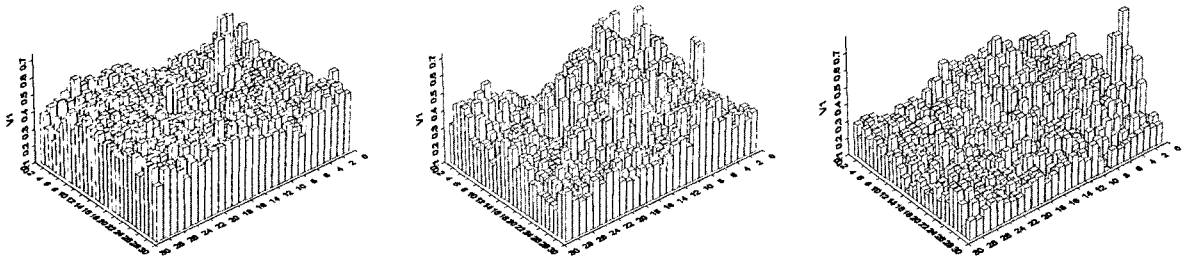

Fig. 8. Three-Dimensional Block Diagram of Case 2 (left: Grass, middle: Soil, right: Manmade).

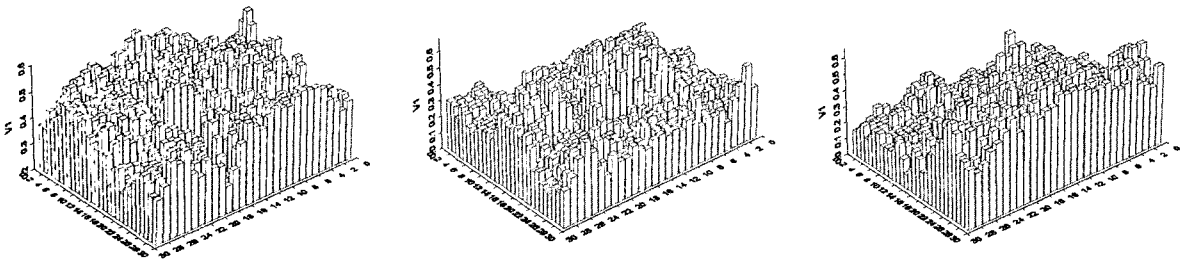

Fig. 9. Three-Dimensional Block Diagram of Case 3 (left: Forest, middle: Soil (or Bright Concrete), right: Manmade).

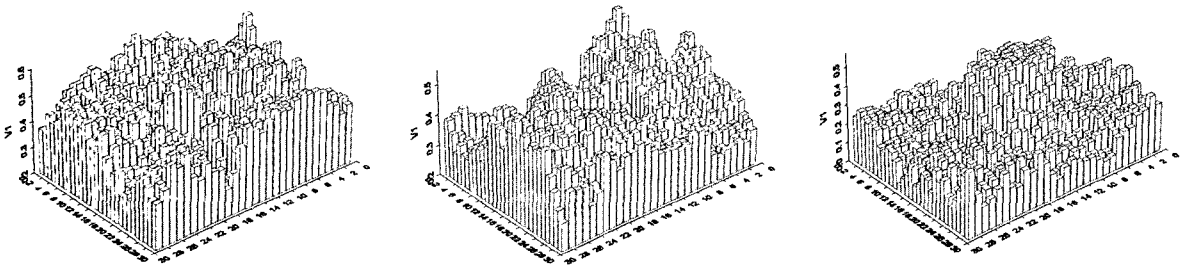

Fig. 10. Three-Dimensional Block Diagram of Case 4 (left: Forest, middle: Grass, right: Water).

Table 3. Values of the Abundance and Image Coordinates (left: Case 1, Light: Case 2).

	Water	Soil	Manmade	RMSE		Grass	Soil	Manmade	RMSE
Abundance (Max.)	0.505	0.522	0.487	0.041		0.734	0.797	0.724	0.006
Image Coordination	(28, 25)	(15, 17)	(26, 3)	(30, 9)		(10, 8)	(24, 19)	(22, 2)	(29, 8)
Abundance (Min.)	0.165	0.249	0.158	0		0.098	0.105	0.009	0
Image Coordination	(25, 7)	(15, 1)	(11, 29)	-		(22, 2)	(22, 2)	(23, 15)	-

Table 4. Values of the Abundance and Image Coordinates (left: Case 3, Light: Case 4).

	Forest	Soil	Manmade	RMSE	Forest	Grass	Water	RMSE
Abundance (Max.)	0.665	0.677	0.655	0.007	0.604	0.548	0.574	0.004
Image Coordination	(8, 1)	(17, 17)	(13, 30)	(12, 12)	(2, 16)	(19, 27)	(18, 17)	(14, 7)
Abundance (Min.)	0.068	0.101	0.034	0	0.156	0.226	0.008	0
Image Coordination	(15, 17)	(8, 20)	(11, 14)	-	(12, 8)	(15, 14)	(3, 15)	-

This implies that it is not a piece of information that needs to be assessed. Lastly, it is our goal to demonstrate that the results of sub-pixel analysis produce more effective information compared with the image classification by focusing on the interest classes.

5. Conclusion

In this paper, we examined one of the sub-pixel analysis algorithms, LSM model, and also discussed about the test performed on the Hyperion data. To find endmembers, we applied the convex geometry on the two-dimensional scatter plot. Atmospheric Correction and Minimum Noise Fraction techniques were used in the pre-processing of the Hyperion Data.

The results of the sub-pixel analysis of some objects were satisfactory. Although the shape of the object couldn't be extracted, we could still assume that the possibility of material existence can be identified in one pixel.

In this study, we detected some limitations of the LSM model. First, in practice the sum of abundance is not unit value, and there exists negative value as well. We also found that the best way to resolve this problem is to run the algorithm iteratively by using the RMS error image. Second, we found that the endmembers play an important role in solving the LSM model. Therefore, the study on the endmember determination must be further improved in order to obtain better results of sub-pixel analysis.

Based on the basic understanding of the limitation of the LSM model, we plan to conduct further studies on the following topics: the endmember determination, detailed processing for sub-pixel analysis, and constrained calculation of abundance.

Acknowledgements

The authors thank the Research Institute of Engineering Science, Seoul National University for their support and the ETRI (Electronics and Telecommunications Research Institute) for providing the Hyperion for this study.

References

1. Antonio Plaza, Pablo Martinez, Rosa Perez, and Javier Plaza (2002). "Spatial/Spectral Endmember Extraction by Multidimensional Morphological Operations", IEEE Transactions on Geoscience and Remote Sensing, Vol. 40, No. 9, pp. 2025-2041.
2. Boarman, J. W. (1989). "Inversion of Imaging Spectrometry Data Using Singular Value Decomposition", IGARSS' 89, 12th Canadian Symposium on Remote Sensing, No. 4, pp. 2069-2072.
3. Boarman, J. W. (1993). "Automating Spectral Unmixing of AVIRIS Data Using Convex Geometry Concepts", Summaries of the Fourth Annual JPL Airborne Geoscience Workshop, JPL Pub. 93-26, Vol. 1, Pasadena, CA, pp. 11-14.
4. Chein-I Chang (2003). Hyperspectral Imaging - Techniques for Spectral Detection and Classification, Kluwer Academic/ Plenum Publishers, New York.
5. Chein-I Chang, Shao-Shan Chiang, James A. Smith, and Irving W. Ginsberg (2002). "Linear Spectral Random Mixture Analysis for Hyperspectral Imagery", IEEE Transactions on Geoscience and Remote Sensing, Vol. 40, No. 2, pp. 375-392.
6. Clark RN, Gallagher AN, Swayze GA (1990). "Material Absorption Band Depth Mapping of Imaging Spectrometer Data Using the Complete Band Shape Least-Squares Algorithm Simultaneously Fit to Multiple Spectral Features from Multiple Materials", Proceeding of the 3rd AVIRIS Workshop, JPL Publication, 90-54, pp. 176-186.
7. David Landgrebe (2002). "Hyperspectral Image Data Analysis", IEEE Signal Processing Magazine, Vol. 19, Issue 1, pp. 17-28.
8. Dimitris Manolakis, Christina Siracusa, and Gary Shaw (2000). "Hyperspectral Subpixel Target Detection Using the Linear Mixing Model", IEEE Transactions on Geoscience and Remote Sensing, Vol. 39, No. 7, pp. 1392-1409.
9. ENVI Tutorials (2002). Research Systems.
10. Freek D. Van Der Meer, and Steven M. De Jong (2001). Imaging Spectrometry - Basic Principles and Prospective Applications, Kluwer Academic Publishers, Netherlands.
11. Harsanyi JC, and Chang CI (1994). "Hyperspectral Image Classification and Dimensionality reduction: An Orthogonal Subspace Projection Appoarch", IEEE Transactions on Geoscience and Remote Sensing, Vol. 32, pp. 779-785.
12. Kruse FA, Lefkof AB, Boardman JB, Heidebrecht KB,

Shapiro AT, Barloon PJ, and Goetz AFH (1993b). "The Spectral Image Processing System (SPIS)-Interactive Visualization and Analysis of Imaging Spectrometer Data", Remote Sensing of the Environment, No. 44, pp. 309-336.

13. Mazer AS, Martin M, Lee M, and Solomon JE (1988). "Image Processing Software for Imaging Spectrometry Data Analysis", Remote Sensing of the Environment, No. 24, pp. 201-210.
14. Nirmal Keshava and John F. Mustard (2002). "Spectral Unmixing", IEEE Signal Processing Magazine, Vol. 19, Issue 1, pp. 44-57.
15. Richard J. Aspinall, W. Andrew Marcus, Joseph W. Boardman (2002). "Considerations in Collecting, Processing, and Analysing high Spatial Resolution Hyperspectral Data for Environmental Investigations", Journal of Geograhpical Systems, No. 4, pp. 15-29.